Title	Harvesting electromagnetic energy in the V-band using a rectenna formed by a bow tie integrated with a 6-nm-thick Au/HfO2/Pt metal-insulator-metal diode
Authors	Aldrigo, Martino;Dragoman, Mircea;Modreanu, Mircea;Povey, Ian M.;Iordanescu, Sergiu;Vasilache, Dan;Dinescu, Adrian;Shanawani, Mazen;Masotti, Diego
Publication date	2018-05-22
Original Citation	Aldrigo, M., Dragoman, M., Modreanu, M., Povey, I., Iordanescu, S., Vasilache, D., Dinescu, A., Shanawani, M. and Masotti, D. (2018) 'Harvesting Electromagnetic Energy in the V -Band Using a Rectenna Formed by a Bow Tie Integrated With a 6-nm-Thick Au/HfO2/Pt Metal–Insulator–Metal Diode', IEEE Transactions on Electron Devices, 65(7), pp. 2973-2980. doi: 10.1109/TED.2018.2835138
Type of publication	Article (peer-reviewed)
Link to publisher's version	https://ieeexplore.ieee.org/document/8362794 - 10.1109/TED.2018.2835138
Rights	© 2018 IEEE. Personal use of this material is permitted. Permission from IEEE must be obtained for all other uses, in any current or future media, including reprinting/republishing this material for advertising or promotional purposes, creating new collective works, for resale or redistribution to servers or lists, or reuse of any copyrighted component of this work in other works.
Download date	2025-05-24 03:42:21
Item downloaded from	https://hdl.handle.net/10468/9756

University College Cork, Ireland
Coláiste na hOllscoile Corcaigh

Harvesting Electromagnetic Energy in the *V*-Band Using a Rectenna Formed by a Bow Tie Integrated With a 6-nm-Thick Au/HfO_2/Pt Metal–Insulator–Metal Diode

Martino Aldrigo, Mircea Dragoman, Mircea Modreanu, Ian Povey, Sergiu Iordanescu, *Member, IEEE*, Dan Vasilache, Adrian Dinescu, Mazen Shanawani, and Diego Masotti, *Senior Member, IEEE*

***Abstract*— In this paper, the first demonstration of a bow-tie antenna integrated with a metal–insulator–metal (MIM) diode for electromagnetic energy harvesting in the *V*-band (i.e., 40–75 GHz) is presented. We have designed, simulated, fabricated, and fully characterized a 60-GHz rectifying antenna (rectenna) based on a vertical Au-HfO_2-Pt MIM diode with reduced differential resistance. The dielectric used for the MIM structure is a 6-nm-thick amorphous HfO_2 grown by atomic layer deposition. For the fabricated MIM device, we report here a current density of 3×10^4 A/cm^2 that exceeds the previous values presented in the literature. The vertical MIM-based rectenna is able to efficiently harvest up to 250 μV from an impinging modulated millimeter-wave signal with −20 dBm of available power, thus offering a voltage responsivity of over 5 V/W. The reported results indicate that the proposed approach is well suited for future low-power solutions much sought after for the energetically autonomous 5G terminal equipment.**

***Index Terms*— Diodes, energy harvesting, millimeter-wave (mm-wave) devices, rectennas.**

I. Introduction

IN THE Internet of Things (IoT), billions of objects are interconnected among them via multiple wireless systems, which are working in different bandwidths. The 5G wireless communications are the backbone of IoT working in the range 1–100 GHz, but some bands are of utmost importance, such as 2.5, 28, or 60 GHz. It is difficult to imagine that billions of "things" (i.e., interconnected devices) will be powered by batteries, which should be charged and replaced often. Therefore, the self-powering functionality is a must for the development of IoT of the future, as envisaged by the 5G multi-tier network architecture [1], thus paving the way to future 5G IoT scenarios [2]–[5]. The self-powering mechanism is based on the available energy in the environment and one of them is the electromagnetic energy of the wireless networks, which is delivered continuously and nearly wasted when the objects are in sleeping mode. Therefore, the electromagnetic energy harvesting at microwave and millimeter waves (mm-waves) is an active research area to solve a thorny issue—the self-powering of objects in IoT [6], [7]. The electromagnetic energy harvesting in microwaves and mm-waves implies various antennas geometries, but all must be equipped with a diode able to rectify the electromagnetic field at zero bias. Such antennas integrated with a diode are termed as "rectennas." Rectennas were originally developed to transform the solar energy into dc having a similar role as solar cells [8]. A recent review and the history of rectennas lasting half of century are reported in [9]. Schottky diodes integrated with various antenna shapes and geometries are used for microwaves and mm-waves harvesting devices, allowing direct CMOS integration [10] up to 95–100 GHz (*W*-band) [11]. New materials are used for Schottky diodes included in rectennas. For instance, Schottky diodes based on diamond are used for high-power rectennas [12], while Schottky diodes based on graphene on doped semiconductors are used for terahertz (THz) harvesting [13]. Moreover, various substrates are used today beyond semiconductors, especially for high-frequency applications in the low region of the microwave spectrum such as paper [14], [15] or textiles [16]. Even metamaterials loaded with diodes are used for efficient harvesting in the 900-MHz band [17]. A review about these new trends in electromagnetic harvesting can be found in [18].

Rectennas can harvest electromagnetic energy also in the optical spectrum. Here, the used diodes are of the metal–insulator–metal (MIM) type, since they are the only electronic

Manuscript received March 29, 2018; accepted May 6, 2018. This work was supported by the European Union's Horizon 2020 research and innovation program under ASCENT Grant 654384. The review of this paper was arranged by Editor R. Venkatasubramanian. *(Corresponding author: Martino Aldrigo.)*

M. Aldrigo, M. Dragoman, S. Iordanescu, and D. Vasilache are with the Micromachined Structures, Microwave Circuits and Devices Laboratory (RF-MEMS), National Institute for Research and Development in Microtechnologies, 077190 Voluntari, Romania (e-mail: martino.aldrigo@imt.ro; mircea.dragoman@imt.ro; sergiu.iordanescu@imt.ro; dan.vasilache@imt.ro).

M. Modreanu and I. Povey are with the Tyndall National Institute, University College Cork, T12 R5CP Cork, Ireland (e-mail: mircea.modreanu@tyndall.ie; ian.povey@tyndall.ie).

A. Dinescu is with the Nano-Scale Structuring and Characterization Laboratory, National Institute for Research and Development in Microtechnologies, 077190 Voluntari, Romania (e-mail: adrian.dinescu@imt.ro).

M. Shanawani and D. Masotti are with the Department of Electrical, Electronic and Information Engineering, University of Bologna, 40136 Bologna, Italy (e-mail: mazen.shanawani@unibo.it; diego.masotti@unibo.it).

Color versions of one or more of the figures in this paper are available online at http://ieeexplore.ieee.org.

Digital Object Identifier 10.1109/TED.2018.2835138

devices able to work in the visible and infrared spectra [19]. MIM diodes are tunneling devices with a cutoff frequency limited only by the tunneling time, i.e., few femtoseconds. However, to attain such high cutoff frequencies, the roughness of the dielectric and metals must be within 0.2–0.3 nm, which is rather difficult to obtain [20]. In the absence of this low roughness, the quantum tunneling becomes less efficient and low current values are expected.

In this respect, we have reported here novel rectennas that can be fabricated at the wafer level using standard microelectronics technologies. We are targeting an operating frequency of 60 GHz for the rectennas as this is a band that was allocated to the IoT. Our rectennas are formed by a bow-tie antenna integrated with an Au/HfO_2/Pt MIM diode for 60-GHz electromagnetic harvesting, this solution being fully CMOS compatible with the rest of circuits integrated in an interconnected object. Amorphous atomic layer deposition (ALD) HfO_2 thin films are the gate dielectric of choice in all current CMOS technologies and offer atomically smooth surface roughness (i.e., attaining 0.1–0.2 nm) that are a prerequisite for high performance MIM devices. The top and down electrodes of the HfO_2 MIM diode form the bow-tie antenna arms.

In Section II, we present the design and simulation details of the proposed rectenna. Section III gives an outlook on the fabrication and dc characterization. Finally, Section IV is dedicated to the high-frequency measurements of the rectenna, with the experimental proof of its harvesting capabilities. Conclusions will follow in Section V.

II. Design and Simulation of the *V*-Band Rectenna

As mentioned in Section I, 60 GHz is one of the bands allocated to IoT. As demonstrated in [21], this frequency could be profitably used for near-range wireless communications with high data rate (up to 2450 Mb/s), at a maximum transmitter–receiver distance of 5–10 cm (which is the distance considered in this paper), with a transmitted power spanning -10 to 10 dBm for bit error rate (BER) values not exceeding 5×10^{-4}. Such a system could be a practical source for the device that we propose, which would be suitable to feed a low-power sensor. In [22], the tag demonstrates power harvesting from the reader transmission with CMOS rectifier at 60 GHz. Hence, in the authors' opinion, despite the well-known propagation losses arising at the mm-waves, the energy harvesting at 60 GHz is a promising approach to be followed as it offers a scalable route for future miniaturization, high data rate and BER reduction in near-range communications. In this respect, we chose as radiating element a bow-tie antenna, which is largely deployed in high-frequency applications due to its large effective area (which increases its radiation efficiency) and high input impedance. In detail, the two radiating arms of a bow tie are excited in a dipole-like configuration, and thus the gap between them becomes an ideal location for the MIM diode. Moreover, a bow tie has a much larger bandwidth than a dipole antenna, and its planar and simple geometry makes it the ideal candidate

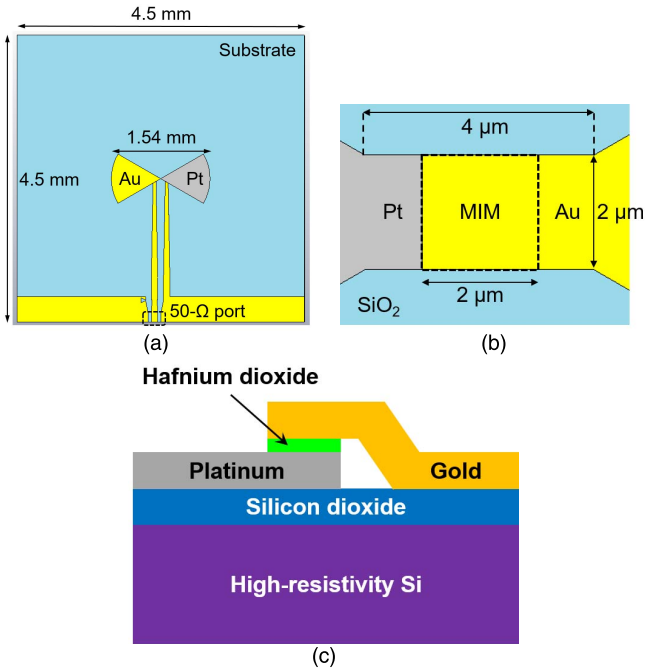

Fig. 1. CST Microwave Studio design (with main dimensions) of (a) top-view of the bow-tie antenna and (b) MIM area in correspondence of antenna's gap. (c) Schematic cross section of the MIM diode and of the substrate.

for high-frequency detection/energy-harvesting applications. These facts have been already demonstrated at much higher frequencies, i.e., in THz- and IR-band applications [23]. The following criteria are adopted: 1) a wide operating bandwidth in the mm-wave frequency range; 2) MIM with different metal contacts to increase diode's asymmetry; 3) a simple solution for the balun circuitry, necessary for this type of antennas; and 4) an optimal matching to a standard 50-Ω input impedance, in coplanar waveguide (CPW) technology.

Rounded edges of the bow-tie antenna are used such that the path length from the feed point to the edge of the bow tie is the same in all directions, thus suppressing some higher order modes and obtaining flatter frequency response than that of the conventional (i.e., triangular) bow tie [24]. In Fig. 1(a) and (b), we show the CST Microwave Studio top-view design (with main dimensions) of the proposed antenna and MIM area, respectively, whereas in Fig. 1(c) we give a schematic cross section of the MIM diode, in which the thin HfO_2 layer is the diode's dielectric and has an overall area of about 4 μm^2, with a theoretical thickness of 6 nm.

The total area occupied by the antenna is 20.25 mm^2, and the bow-tie antenna has a total length of about 1.54 mm. The substrate consists of high-resistivity silicon (HR Si) with a thickness of 525 μm, over which there is a 300-nm-thick film of silicon dioxide (SiO_2). The feeding port was designed in CPW technology, with a gap-signal-gap configuration of 60–100–60 μm that guarantees an input impedance of 50 Ω.

As regards the modeling inputs for the HfO_2 dielectric, we like to stress here that the reported dielectric characteristics of HfO_2 thin films are known up to 20 GHz [25], [26], with average permittivity values spanning mostly in the range 18–22 and a loss tangent of maximum 10^{-1}.

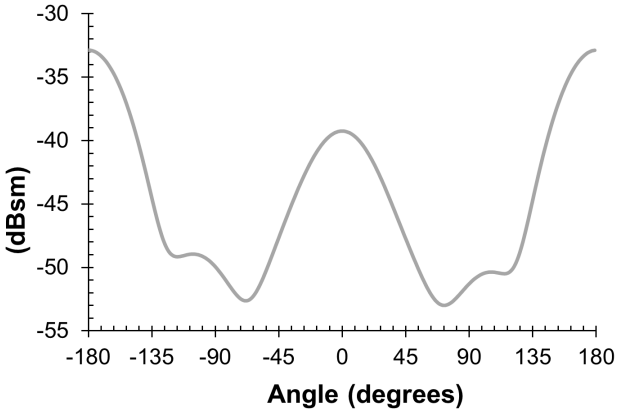

Fig. 2. Bistatic scattering RCS on the horizontal plane (i.e., perpendicular to the plane of the antenna) at 60 GHz for different values of the angle (ϑ).

Finally, we have designed a symmetric coplanar stripline (CPS) and the relative CPW-to-CPS transition, in order to feed the bow-tie antenna without an *ad hoc* balun. The balun (i.e., balance–unbalanced device) is a component used in all cases in which a transition from a balanced (our antenna, in the present case of study) to an unbalanced (i.e., the CPW port) signal is required. The abovementioned transition is realized also by means of an inverse triangular stub: in this respect, it is important to keep the total stub length as short as possible, if wider bandwidths are required. Furthermore, the stub is very useful for two main purposes: 1) matching to 50 Ω and 2) widening the bandwidth (since it is a short-circuit stub with an inductive reactance, thus canceling the capacitive load of the MIM diode). Thus, we can expect an antenna input impedance optimized on a standard 50-Ω port.

In Fig. 2, we show the simulated bistatic scattering radar cross section (RCS) on the horizontal plane (i.e., perpendicular to the plane of the antenna) at 60 GHz when exciting the bow tie with a plane wave (this is the usual situation in a detection/harvesting application). In correspondence of the maximum direction ($\vartheta = 0°$), the RCS is -39.25 dBsm (i.e., dB square meter, as defined by the electromagnetic simulator). Furthermore, the 3-dB angular width with respect to the direction of maximum is equal to 50° (i.e., $\vartheta \in [-25°, 25°]$), which means that the backscattered signal is consistent in a quite wide range of values. This result is of outmost importance, since we can expect an efficient detection/absorption of the incoming signal in the mm-wave frequency range. This is reflected also in the simulated radiation efficiency and gain, which are about 79% and about 4 dBi (a typical value for bow-tie antennas), respectively. The return loss (i.e., $|S_{11}|$ parameter) is also simulated, showing values less than -10 dB in the bandwidth 61–65 GHz, which is typical for a wideband antenna like the bow tie.

III. Fabrication and DC Characterization of the *V*-Band Rectenna

The MIM structure is fabricated on thermally oxidized (300-nm-thick SiO_2) HR Si (100) substrate. The optimal solution found for the rectenna is as follows: the bottom MIM

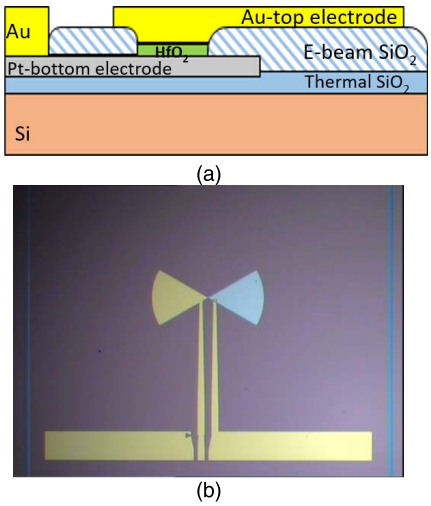

Fig. 3. (a) Schematic cross section of the MIM diode fabrication process. (b) Optical image of the rectenna.

electrode is made of 150-nm-thick sputtered Pt configured by dry etch; an isolation layer of 100-nm-thick E-beam SiO_2 is configured by a lift-off process to open the area where the 6-nm-thick HfO_2 is deposited by ALD. The thickness of HfO_2 thin films was first measured by spectroscopic ellipsometry [27], and then further on it was confirmed by the TEM measurements. The TEM results outline the amorphous nature of 6-nm-thick HfO_2 thin films. The ALD precursors use for the growth of HfO_2 thin films were Tetrakis (ethylmethylamido)-hafnium (TEMAHf) and water, with an ALD growth temperature of 200 °C; finally, another lift-off process was used for configuring the top electrode, 300-nm-thick Au deposited by sputtering with an adhesion layer of 20-nm-thick Ti. The Pt and Au electrodes are the bottom and top electrodes of the MIM and are in the shape of the bow-tie antenna. Batches of twenty rectennas have been fabricated on the same HR Si wafer. The cross section of the fabrication flow developed for the MIM diode coupled to the bow-tie antenna is outlined in Fig. 3(a), while the optical image of the rectenna is presented in Fig. 3(b). Fig. 4(a) is the SEM image of the MIM area of the rectenna, and Fig. 4(b) is a TEM image of the MIM.

After the fabrication, the MIM diodes are first measured using a Keithley 4200 SCS equipment. The I–V dependence shows an exponential behavior, the current density being calculated considering an MIM area of 40×10^{-9} cm^2. At 0 V, there is a small leakage current of -900 nA, which is four orders of magnitude lower than the maximum measured dc current. The values of currents obtained are 20 000× times bigger than those obtained for Ni/NiO/Ni MIM diodes [28] and 12.5× times bigger than the measured Cr/Al_2O_3-HfO_2/Cr MIM presented in [29]. These high current values in a small voltage range have a major impact on the MIM-coupled-antenna system, namely, a strong reduction of diode's differential resistance R_D, which is defined as follows:

$$R_D = 1/(\partial I/\partial V). \tag{1}$$

From the I–V curve, we can extract a maximum measured value for $R_{D0} = R_D(V = 0)$ of about 405 Ω, whereas at ±100 mV we have $R_D \approx 300$ Ω (average value), and at

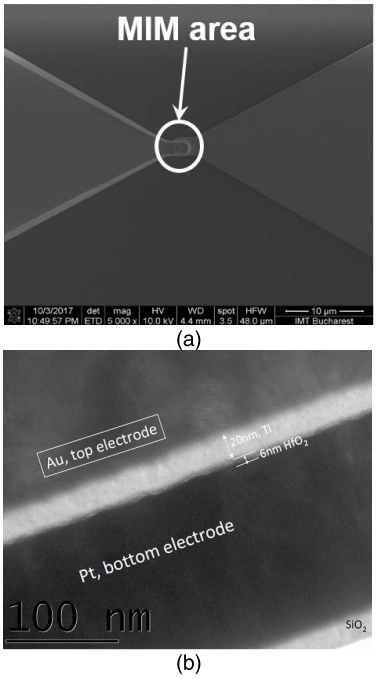

Fig. 4. (a) SEM image of the MIM area of the rectenna. (b) TEM image of the MIM diode.

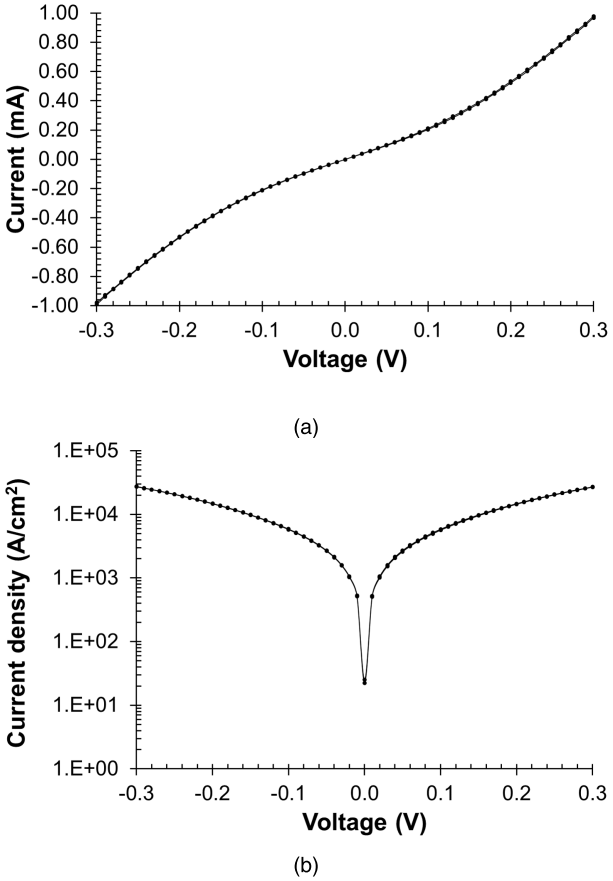

Fig. 5. (a) Measured I–V dependence. (b) Current density (in A/cm^2) of the MIM diode in the ±300 mV voltage range.

±300 mV, we obtain $R_D \approx 92\ \Omega$ (average value). Since the bow-tie input impedance is around 300 Ω, it is evident how the proposed device guarantees an ideal coupling to antenna's characteristic impedance even in 0-V bias conditions and up to ±100 mV. Furthermore, the static capacitance of the MIM diode is $C_{\mathrm{MIM}} \approx 99.88$ fF (considering that $\varepsilon_{\mathrm{HfO2}} = 20$), which corresponds to a reactance $X_{\mathrm{MIM}} \approx -26\ \Omega$ around 60 GHz. The I–V dependences are similar for many measured MIM diodes and are represented in Fig. 5(a) and (b).

In Fig. 6(a) and (b), we show two important figures of merit for MIM diodes in mm-wave and THz rectenna applications [30], namely, nonlinearity χ and curvature coefficient (or sensitivity) γ, which are defined as follows:

$$\chi = (\partial I/\partial V)/(I/V) \tag{2}$$

$$\gamma = (\partial^2 I/\partial V^2)/(\partial I/\partial V). \tag{3}$$

In particular, $\chi \approx 2.1$ at ±300 mV, with a sensitivity $\gamma = -6.263\ \mathrm{V}^{-1}$ at −156 mV and $\gamma = 6.583\ \mathrm{V}^{-1}$ at 148 mV. The latter values are beyond the state-of-the-art present in the literature, where a value of γ not exceeding 5 V^{-1} can be found [23], [28], [29].

We have also estimated the noise-equivalent power (NEP) for the HfO_2-based rectenna, which is NEP = 471 pW/Hz$^{0.5}$, hence a very good value with respect to state-of-the-art detectors with nanomaterials [31].

IV. High-Frequency Measurements

We have measured the devices on a 9-mm-thick Plexiglas support and on a metal plate, to evidence possible discrepancies between the two situations. However, as we will see in the following, no significant differences have been observed between the two supports, thus having a proof of the fact that the rectennas could be exploited disregarding the backing material (i.e., either dielectric or conductor). Fig. 7 displays the comparison between simulated and measured antenna input impedance Z_{11} (real and imaginary parts—$\mathrm{Re}\{Z_{11}\}$ and $\mathrm{Im}\{Z_{11}\}$, respectively) of the HfO_2-based mm-wave rectenna, whereas in Fig. 8 the simulated and measured return loss are reported. We have carried out measurements in the 40–100-GHz band by using an Anritsu 37397D vector network analyzer.

We stress here that the frequency of 61.6 GHz was chosen after systematic RF measurements in the 55–65-GHz band, meant to search for the frequency at which the harvested signal was maximum. From Fig. 7, at 61.6 GHz, the measurements show $\mathrm{Re}\{Z_{11}\} = 41.52\ \Omega$, whereas $\mathrm{Im}\{Z_{11}\} = -4.75\ \Omega$ (which corresponds to a slightly capacitive reactance). In particular, from the simulated $\mathrm{Im}\{Z_{11}\}$ we expected to have a resonance (in correspondence of which $\mathrm{Im}\{Z_{11}\} = 0\ \Omega$) around 61.2 GHz, so that the reference frequency of 61.6 GHz can be considered very close to the predicted value for optimal impedance matching and maximum radiation.

The noise around the operating frequency was due to the measurement setup calibration and could not be avoided. One can notice that the antenna is wideband, since the variation of $|S_{11}|$, with respect to $|S_{11}|$ values far from the targeted frequency range, is better than 10 dB within the 61–65 GHz band. This aspect, particularly crucial to maximize the power

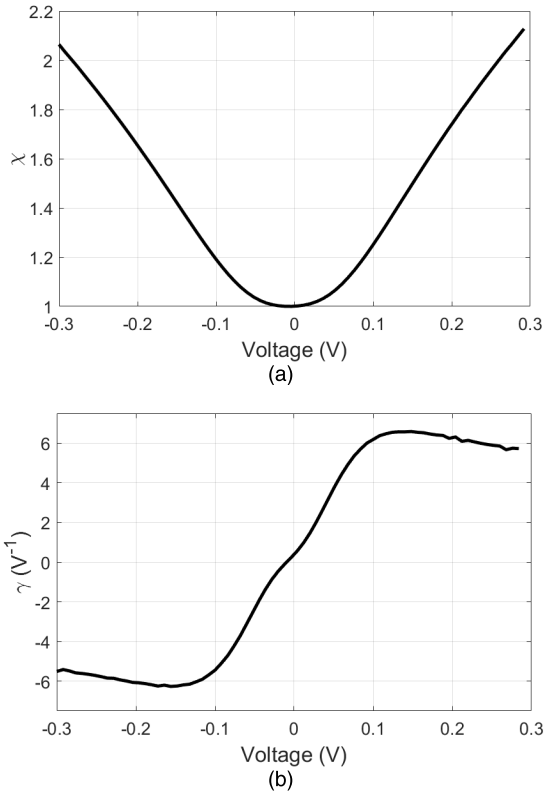

Fig. 6. Extracted (a) nonlinearity χ and (b) sensitivity γ of the measured MIM diode.

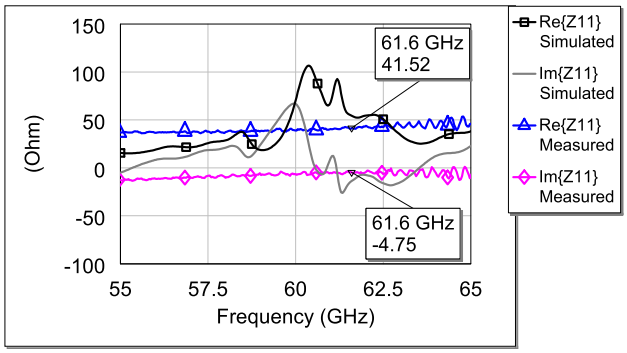

Fig. 7. Comparison between measured and simulated input impedance (real and imaginary parts) of the rectenna.

transfer from the antenna to the measurement port, could be explained by considering (as mentioned in the previous paragraphs) that antenna input impedance has a real part $R_A \approx 50 \pm 10\ \Omega$, whereas its imaginary part $X_A \to 0\ \Omega$ all over the band of interest. In this respect, a clear proof is given by the flat response in frequency of antenna input impedance: this justifies the very good matching to 50 Ω at the operating frequency. In fact, the measured value of $|S_{11}|$ at 61.6 GHz is −19.5 dB, whereas the simulated one is −17.32 dB (see Fig. 8). In spite of the lack of an evident resonance peak in the measurements of return loss, the fact that the maximum radiation occurs very close to the predicted (simulated) frequency (i.e., 61.2 GHz, as stated before) is a clear proof that the rectenna would exhibit a more pronounced resonant behavior (with a minimum of $|S_{11}|$ at 61.6 GHz) if

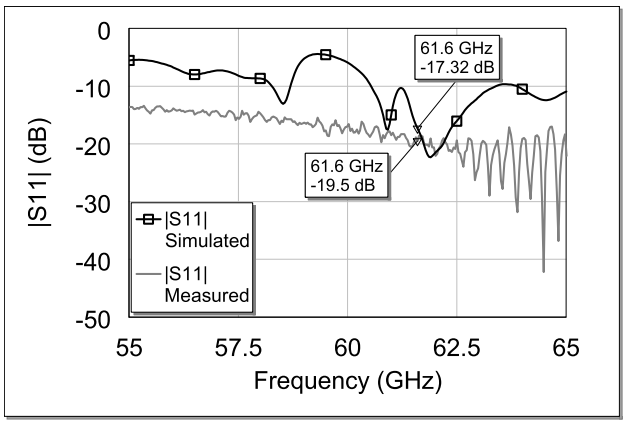

Fig. 8. Comparison between measured and simulated return loss $|S_{11}|$ of the rectenna.

the effect of losses and noise were less significant. Moreover, separating linear and nonlinear effects within the diode, would yield just a little accuracy improvement at this high power level, and the only accurate solution is that of self-consistent simulations, which is not accounted to be the electromagnetic simulator.

The good matching is further improved by the presence of the inverse stub in correspondence of the CPW–CPS transition, which cancels the (capacitive) reactive part of the MIM diode X_{MIM} (with $X_{\mathrm{MIM}} \approx -26\ \Omega$ around 60 GHz). Hence, we can expect to be in the ideal situation of optimal antenna-to-diode matching at the targeted frequency, thus significantly enhancing the power transfer from the antenna to the measurement port. The device losses can be related to thin-conductor loss phenomena. In fact, the Pt electrode has a thickness that is half of the skin-effect depth at 61.6 GHz; nevertheless, it was a technological constraint to have a thin metallization in order to guarantee a low roughness for HfO_2 deposition. Other technological issues regarding the deposition of the thin HfO_2 layer could be responsible for the discrepancies between simulated and measured $|S_{11}|$, for example, the fact that the contact area is slightly different [i.e., $(1.9 \pm 0.1) \times (1.9 \pm 0.1)\ \mu\mathrm{m}^2$] and thinner (i.e., about 6 nm instead of 10 nm) than the simulated ones; the real value of HfO_2 permittivity is also affected by uncertainties (since it spans in the range 18–22, as stated in Section II). All the latter issues have a great influence on the effective diode's capacitance and, hence, on the experimental characterization as well.

The setup to characterize the rectenna properties is depicted in Fig. 9. We used an Agilent E8257D PSG Analog Signal Generator (band 250 kHz–50 GHz) set to provide a 15.4-GHz sinusoidal carrier. It was connected to the 4× frequency multiplier S15MS-AG 50 to 75-GHz Millimeter-Wave Source Module, so as to give an output carrier at 61.6 GHz. The signal generator has an output power of 17 dBm, whereas the fixed output power of the multiplier is 10 dBm. The 61.6-GHz carrier was modulated by an AM square signal, with rate of 1 kHz and depth of 100%. We chose to use an AM modulation in order to verify the effective harvesting capabilities of the proposed rectenna in presence of a signal other than a simple mm-wave carrier. Furthermore, the usage of a sequence of

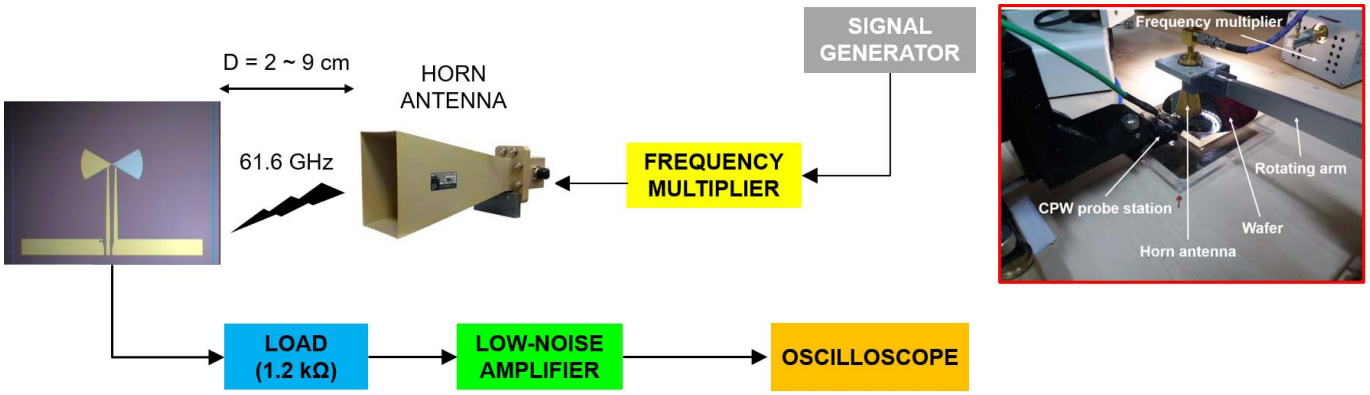

Fig. 9. Rectenna measurement setup for high-frequency characterization. Inset: a picture with the main components is displayed.

square pulses (due to the 100% depth of the modulating signal) was useful to emphasize the detection itself. Since the MIM diode does not have a threshold voltage (like in the case of Schottky diodes) and exhibits conduction for both negative and positive values of the applied voltage, we expected to observe a detected signal following the input modulation. The transmitting antenna is a standard-gain horn antenna, with bandwidth from 50 to 75 GHz and gain of 20 dBi. It was placed at a distance D between 2 and 9 cm from the rectenna. Considering that the maximum linear dimension $L_{\max}$ of the bow tie is 1.54 mm, for a free-space wavelength $\lambda_0 \approx 4.87$ mm (at 61.6 GHz) the horn antenna was in the far-field (or Fraunhofer) region of the bow tie if $D > 2L_{\max}^2/\lambda_0$. In our case, $2L_{\max}^2/\lambda_0 \approx 1$ mm, so that the far-field prerequisite was satisfied at every distance considered in our measurements. This guarantees the correct excitation of the antenna in realistic working conditions. We will refer to the horn antenna as "transmitter." The rectenna load was provided by the coaxial cables and by a 1.2-kΩ load, as shown in Fig. 9. As regards the low-noise amplifier (LNA), it is an SRS Stanford Research Systems, model SR560. The chosen "gain mode" was "low noise," with gain = 1000 and a 6 dB/oct rolloff low-pass filter with cutoff of 10 kHz, dc coupling to antenna output and the port connecting the antenna to the LNA with an impedance of 100 MΩ + 25 pF, whereas the output to the oscilloscope is a port with a 600-Ω impedance. It was necessary to use an LNA since we expected to have, as stated before, sub-millivolts detected signals, which otherwise could not be observed with the oscilloscope (having a resolution of minimum 1 mV). We used a Tektronix DPO 2024 Digital Oscilloscope to detect the signal output from the antenna (and amplified by the LNA).

Fig. 10(a) shows the results of the high-frequency measurements performed on the proposed HfO_2-based mm-wave rectenna, whereas Fig. 10(b) is the measured voltage responsivity as a function on the incident power. In detail, Fig. 10(a) demonstrates how the amplitude of the time-dependent detected voltage V_{det} follows the AM-modulated input signal (in fact, two consecutive peaks are at a distance of 1 ms, which is in agreement with the 1 kHz rate of the AM modulation), with decreasing amplitude as the distance of the transmitter from the bow tie increases, namely, from 5λ up to 18λ. After this threshold, the detected voltage is very weak

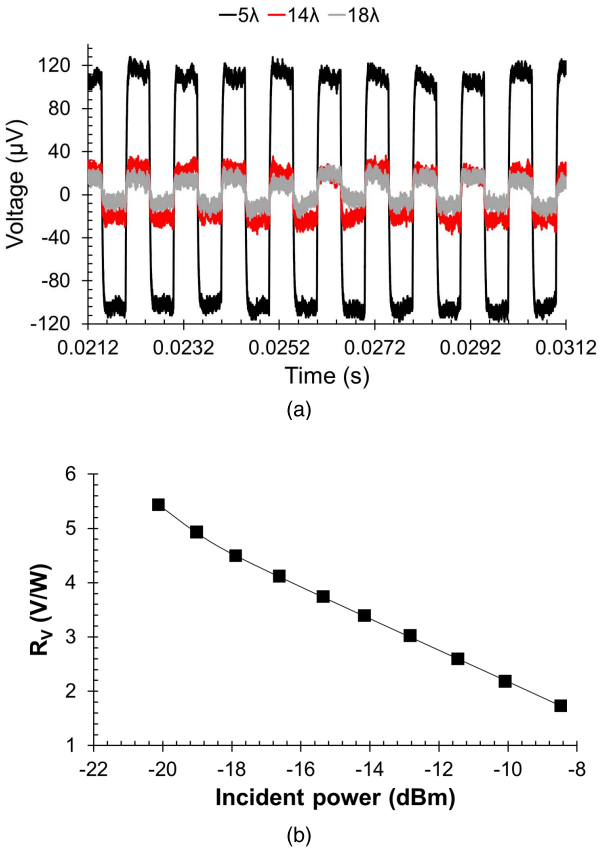

Fig. 10. (a) Time response of the rectenna for a modulated excitation at 61.6 GHz. (b) Extracted responsivity as a function of the incident power.

and the oscilloscope noise predominates. All the measured devices provided similar performance. The successive device improvement will take into account also the optimal values of the RC load circuit, able to further enhance the detected voltage.

As regards the voltage responsivity R_V (in V/W), we calculated the power incident onto the bow-tie antenna by a straightforward application of the Friis formula for the link budget. This way, we can have a clear idea of the effective mm-wave power received by the bow tie. Table I summarizes the main performance of the rectenna.

TABLE I
MILLIMETER-WAVE PERFORMANCE OF THE RECTENNA AS A FUNCTION OF TRANSMITTER DISTANCE *D*

D	V_{det} (peak-to-peak)	Voltage responsivity R_V (V/W)
5λ	~246 μV	5.432
14λ	~73.2 μV	4.496
18λ	~52.8 μV	1.729

V. CONCLUSION

In this paper, we have presented the design, modeling, fabrication, and full dc/mm-wave characterization of an mm-wave HfO_2-based rectenna. We have designed a 61.6-GHz bowtie antenna, coupled to an HfO_2 MIM diode, and efficiently matched to a standard 50-Ω CPW port. The detailed fabrication process has been provided, together with potential issues that need to be solved for further technological improvements. The potentialities of the HfO_2-based rectenna has been proven by measuring the MIM I–V characteristic, which shows a much higher current with respect to current state-of-the-art, lower resistance (i.e., hundreds of Ω) and high robustness against mechanical, electrical, and thermal stress. The final mm-wave characterization has fully demonstrated the detection capabilities of the fabricated device, with a peak-to-peak detected voltage of almost 250 μV at a distance of 5λ from the mm-wave transmitter and a voltage responsivity of 5.432 V/W for an incident power of about −20 dBm. The proposed HfO_2-based mm-wave rectenna can be considered in reason as a promising candidate for easy-to-embed detectors/energy harvesters for the emerging 5G technology.

From a practical point of view, the energy transfer to a low-power sensor (a potential candidate to be integrated with the harvester proposed in this paper) could be realized in a straightforward way by deploying a 60-GHz harvester array, hence combining the output of a certain number of MIM-based single harvesters, at the expense of a reduced occupied area (for example, a 4 × 4 array would occupy only 9 × 9 mm^2). This way, a dc voltage of up to some millivolts could be extracted and used to supply an energetically autonomous electronic device. This topic will be the object of future research in the domain of integrated mm-wave energy harvesters.

ACKNOWLDGMENT

The authors would like to thank the Nanoelectronics Fabrication Team at Tyndall National Institute, Cork, Ireland.

REFERENCES

[1] E. Hossain, M. Rasti, H. Tabassum, and A. Abdelnasser, "Evolution toward 5G multi-tier cellular wireless networks: An interference management perspective," *IEEE Wireless Commun.*, vol. 21, no. 3, pp. 118–127, Jun. 2014. [Online]. Available: https://doi.org/10.1109/MWC.2014.6845056

[2] D. Bandyopadhyay and J. Sen, "Internet of Things: Applications and challenges in technology and standardization," *Wireless Pers. Commun.*, vol. 58, no. 1, pp. 49–69, 2011. [Online]. Available: https://doi.org/10.1007/s11277-011-0288-5

[3] M. R. Palattella *et al.*, "Internet of Things in the 5G era: Enablers, architecture, and business models," *IEEE J. Sel. Areas Commun.*, vol. 34, no. 3, pp. 510–527, Mar. 2016. [Online]. Available: https://doi.org/10.1109/JSAC.2016.2525418

[4] O. Galinina, H. Tabassum, K. Mikhaylov, S. Andreev, E. Hossain, and Y. Koucheryavy, "On feasibility of 5G-grade dedicated RF charging technology for wireless-powered wearables," *IEEE Wireless Commun.*, vol. 23, no. 2, pp. 28–37, Apr. 2016. [Online]. Available: https://doi.org/10.1109/MWC.2016.7462482

[5] A. Costanzo and D. Masotti, "Energizing 5G: Near- and far-field wireless energy and data trantransfer as an enabling technology for the 5G IoT," *IEEE Microw. Mag.*, vol. 18, no. 3, pp. 125–136, May 2017. [Online]. Available: https://doi.org/10.1109/MMM.2017.2664001

[6] A. Costanzo and D. Masotti, "Smart solutions in smart spaces: Getting the most from far-field wireless power transfer," *IEEE Microw. Mag.*, vol. 17, no. 5, pp. 30–45, May 2016. [Online]. Available: https://doi.org/10.1109/MMM.2016.2525119

[7] L. G. Tran, H. K. Cha, and W. T. Park, "RF power harvesting: A review on designing methodologies and applications," *Micro Nano Syst. Lett.*, vol. 5, no. 1, p. 14, 2017. [Online]. Available: https://doi.org/10.1186/s40486-017-0051-0

[8] G. Moddel and S. Grover, *Rectenna Solar Cells*. Springer, 2013. [Online]. Available: https://doi.org/10.1007/978-1-4614-3716-1

[9] E. Donchev, J. S. Pang, P. M. Gammon, and A. Centeno, "The rectenna device: From theory to practice (a review)," *MRS Energy Sustainab.*, vol. 1, no. e1, pp. 1–34, 2014. [Online]. Available: https://doi.org/10.1557/mre.2014.6

[10] A. Y.-S. Jou, R. Azadegan, and S. Mohammadi, "High-resistivity CMOS SOI rectenna for implantable applications," *IEEE Microw. Wireless Compon. Lett.*, vol. 27, no. 9, pp. 854–856, 2017. [Online]. Available: https://doi.org/10.1109/LMWC.2017.2734776

[11] E. Shaulov, S. Jameson, and E. Socher, "W-band energy harvesting rectenna array in 65-nm CMOS," in *IEEE MTT-S Int. Microw. Symp. Dig.*, Jul. 2017, pp. 307–310. [Online]. Available: https://doi.org/10.1109/MWSYM.2017.8059105

[12] T. Oishi, N. Kawano, and S. Masuya, "Diamond Schottky barrier diodes with NO_2 exposed surface and RF-DC conversion toward high power rectenna," *IEEE Electron Dev. Lett.*, vol. 38, no. 1, pp. 87–90, Jan. 2017. [Online]. Available: https://doi.org/10.1109/LED.2016.2626380

[13] M. Dragoman and M. Aldrigo, "Graphene rectenna for efficient energy harvesting at terahertz frequencies," *Appl. Phys. Lett.*, vol. 109, no. 11, p. 113105, 2016. [Online]. Available: https://doi.org/10.1063/1.4962642

[14] V. Palazzi *et al.*, "A novel ultra-lightweight multiband rectenna on paper for RF energy harvesting in the next generation LTE bands," *IEEE Trans. Microw. Theory Techn.*, vol. 66, no. 1, pp. 366–379, Jan. 2018. [Online]. Available: https://doi.org/10.1109/TMTT.2017.2721399

[15] M. Fantuzzi, D. Masotti, and A. Costanzo, "A novel integrated UWB–UHF one-port antenna for localization and energy harvesting," *IEEE Trans. Antennas Propag.*, vol. 63, no. 9, pp. 3839–3848, Sep. 2015. [Online]. Available: https://doi.org/10.1109/TAP.2015.2452969

[16] S. Lemey, F. Declercq, and H. Rogier, "Textile antennas as hybrid energy-harvesting platforms," *Proc. IEEE*, vol. 102, no. 11, pp. 1833–1857, Nov. 2014. [Online]. Available: https://doi.org/10.1109/JPROC.2014.2355872

[17] A. M. Hawkes, A. R. Katko, and S. A. Cummer, "A microwave metamaterial with integrated power harvesting functionality," *Appl. Phys. Lett.*, vol. 103, no. 16, p. 163901, 2013. [Online]. Available: https://doi.org/10.1063/1.4824473

[18] A. Costanzo *et al.*, "Electromagnetic energy harvesting and wireless power transmission: A unified approach," *Proc. IEEE*, vol. 102, no. 11, pp. 1692–1711, Nov. 2014. [Online]. Available: https://doi.org/10.1109/JPROC.2014.2355261

[19] S. J. Byrnes, R. Blanchard, and F. Capasso, "Harvesting renewable energy from Earth's mid-infrared emissions," *Proc. Nat. Acad. Sci. USA*, vol. 111, no. 11, pp. 3927–3932, 2014. [Online]. Available: https://doi.org/10.1073/pnas.1402036111

[20] E. W. Cowell, III, *et al.*, "Advancing MIM electronics: Amorphous metal electrodes," *Adv. Mater.*, no. 23, pp. 74–78, Jan. 2011. [Online]. Available: https://doi.org/10.1002/adma.201002678

[21] M. Taghivand, K. Aggarwal, Y. Rajavi, and A. S. Y. Poon, "An energy harvesting 22×60 GHz transceiver with scalable data rate of 38–2450 Mb/s for near-range communication," *IEEE J. Solid-State Circuits*, vol. 50, no. 8, pp. 1889–1902, Aug. 2015. [Online]. Available: https://doi.org/10.1109/JSSC.2015.2429716

[22] S. Pellerano, J. Alvarado, and Y. Palaskas, "A mm-wave power harvesting RFID tag in 90 nm CMOS," *IEEE J. Solid-State Circuits*, vol. 45, no. 8, pp. 1627–1637, Aug. 2010. [Online]. Available: https://doi.org/10.1109/JSSC.2010.2049916

[23] M. Bareib *et al.*, "Nano antenna array for terahertz detection," *IEEE Trans. Microw. Theory Techn.*, vol. 59, no. 10, pp. 2751–2757, Oct. 2011. [Online]. Available: https://doi.org/10.1109/TMTT.2011.2160200
[24] S. W. Qu and C. L. Ruan, "Effect of round corners on bowtie antennas," *Prog. Electromagn. Res.*, vol. 57, pp. 179–195, 2006. [Online]. Available: https://doi.org/10.2528/PIER05072103
[25] S. Cimino *et al.*, "A study of the leakage current in TiN/HfO_2/TiN capacitors," *Microelectron. Eng.*, vol. 95, pp. 71–73, Jul. 2012. [Online]. Available: https://doi.org/10.1016/j.mee.2011.03.009
[26] T. T. Vo *et al.*, "*In-situ* microwave characterization of medium-k HfO_2 and High-k STO dielectrics for MIM capacitors integrated in back-end of line of IC," in *Proc. Asia–Pacific Microw. Conf.*, Dec. 2007, pp. 1–4. [Online]. Available: https://doi.org/10.1109/APMC.2007.4555089
[27] M. Modreanu *et al.*, "Investigation of thermal annealing effects on microstructural and optical properties of HfO_2 thin films," *Appl. Surf. Sci.*, vol. 253, pp. 328–334, Oct. 2006. [Online]. Available: https://doi.org/10.1016/j.apsusc.2006.06.005
[28] K. Choi *et al.*, "A focused asymmetric metal–insulator–metal tunneling diode: fabrication, DC characteristics and RF rectification analysis," *IEEE Trans. Electron Devices*, vol. 58, no. 10, pp. 3519–3528, Oct. 2011. [Online]. Available: https://doi.org/10.1109/TED.2011.2162414
[29] P. Maraghechi, A. Foroughi-Abari, K. Cadien, and A. Y. Elezzabi, "Enhanced rectifying response from metal-insulator-insulator-metal junctions," *Appl. Phys. Lett.*, vol. 99, no. 25, pp. 253503-1–253503-3, Dec. 2011. [Online]. Available: https://doi.org/10.1063/1.3671071
[30] M. Shanawani, D. Masotti, and A. Costanzo, "THz rectennas and their design rules," *Electronics*, vol. 6, no. 4, p. 99, 2017. [Online]. Available: https://doi.org/10.3390/electronics6040099
[31] A. Zak *et al.*, "Antenna-integrated 0.6 THz FET direct detectors based on CVD graphene," *Nano Lett.*, vol. 14, no. 10, pp. 5834–5838, 2014. [Online]. Available: https://doi.org/10.1021/nl5027309

Martino Aldrigo received the Ph.D. degree in electronics engineering, telecommunications, and information technology from the Faculty of Engineering, University of Bologna, Bologna, Italy, in 2014.

He is currently a Principal Researcher III with IMT-Bucharest, Voluntari (Ilfov), Romania. He has co-authored more than 50 papers in ISI ranked journals and conferences. His current research interests include the electromagnetic simulation and experimental characterization of RF/microwave/millimeter-wave/terahertz systems for wireless/energy-harvesting applications.

Mircea Dragoman received the Ph.D. degree in electronics from the University "Politehnica," Bucharest, Romania, in 1991.

He is currently a Senior Researcher I with IMT-Bucharest, Voluntari (Ilfov), Romania. He has co-authored more than 250 scientific papers in ISI ranked journals and conferences, and six monographies.

Dr. Dragoman was a recipient of the "Gheorghe Cartianu" prize of the Romanian Academy in 1999.

Mircea Modreanu received the Ph.D. degree (*magna cum laude*) in condensed physics matter from the University of Bucharest, Bucharest, Romania, in 2002.

He is currently a Staff Research Scientist with the Tyndall National Institute, Cork, Ireland. He has authored or co-authored more than 120 papers in the area of materials science and optical spectroscopy of thin films and interfaces.

Ian Povey received the Ph.D. degree in spectroscopic studies of III/V semiconductor growth mechanisms from The University of Manchester, Manchester, U.K., in 1992.

He is currently a Senior Scientist and an Activity Leader for Atomic Layer Deposition with the Tyndall National Institute, University College Cork, Cork, Ireland. He has authored or co-authored more than 150 journal papers in the areas of spectroscopy and materials.

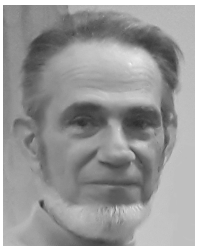

Sergiu Iordanescu (M'91) received the Ph.D. degree in electronic engineering from the University "Politehnica," Bucharest, Romania, in 2000.

He has authored more than 70 scientific papers in peer-reviewed journals and conferences. His current research interests include microwave surface acoustic wave filter, sensor and microwave/millimeter-wave circuits design and characterization, and dielectric and ferroelectric materials characterization.

Dan Vasilache received the Ph.D. degree from the University "Politehnica," Bucharest, Romania.

He is currently a Senior Researcher II with IMT-Bucharest, Voluntari (Ilfov), Romania. He has authored more than 150 articles in ISI ranked journals and conferences. His current research interests include MEMS and NEMS design, manufacturing and encapsulation—thin-film deposition and patterning and masks design and manufacturing.

Adrian Dinescu received the Ph.D. degree in solid-state physics from the Faculty of Physics, University of Bucharest, Bucharest, Romania, in 2010.

He is currently the Head of the Nanoscale Structuring and Characterization Laboratory with IMT-Bucharest, Voluntari (Ilfov), Romania. He has co-authored more than 100 papers in ISI ranked journals. His current research interests include micro- and nanofabrication and optoelectronic measurements.

Mazen Shanawani received the M.Sc. degree (with distinction) in communication systems and signal processing from the University of Bristol, Bristol, U.K. He is currently pursuing the Ph.D. degree in the millimeter and terahetrz rectennas field with the University of Bologna, Bologna, Italy.

He participates to the regional project POR-FESR SINERGIE aiming at using wireless energy transfer concepts at a wider commercial scale.

Diego Masotti (M'00–SM'16) received the Ph.D. degree in electric engineering from the University of Bologna, Bologna, Italy, in 1997.

In 1998, he joined the University of Bologna as a Research Associate of electromagnetic fields. His current research interests include nonlinear microwave circuit simulation and design.

Dr. Masotti serves the Editorial Board of the *International Journal of Antennas and Propagation* and of the *Cambridge journal of Wireless Power Transfer*.